JOINT INSTITUTE FOR NUCLEAR RESEARCH
Dzhelepov Laboratory of Nuclear Problems

FINAL REPORT ON THE
SUMMER STUDENT PROGRAM

Hadronic background study in DsTau experiment

Supervisor: Svetlana Vasina
Student: Sitnikova Elizaveta, Russia Moscow Institute of Physics and Technology
Participation period: July 22 – September 1

Dubna, 2018

Abstract

The aim of the DsTau experiment is a ν_τ production study in 400 GeV/c proton CERN SPS beam via $D_s \rightarrow \tau\nu_\tau$ with subsequent $\tau \rightarrow X\nu_\tau$ decay detection. In total, about 1000 such decays will be detected in $4.6 \cdot 10^9$ protons on target statistics. The main source of background mimicking this decay are secondary hadronic interactions and scattering. In this report the study of charged secondary hadronic interactions in proton beam using the FLUKA-based Monte-Carlo data is presented. In the following study the simulated pion interaction data is compared with existing test beam data for several energies to confirm that the model used in Monte-Carlo is consistent with experimental results and can be used for the background study in DsTau experiment. After that hadronic background is evaluated using different selection criteria. Two approaches to background evaluation were applied: simple rectangular cuts and the likelihood method. Both provide acceptable background level, although the likelihood method allows to reduce background, while maintaining detection efficiency at the same level, as for initially suggested criteria. The likelihood approach significantly increases background suppression for the extended charmed particle study in the DsTau experiment.

Introduction

Neutrino physics is one of the most interesting fields of particle physics. Still there are several open questions, related to this topic, such as oscillation parameters, sterile neutrino existence, neutrino mass hierarchy, CP violation phase, Dirac or Majorana neutrino nature and lepton universality. Tau neutrino is still the least studied elementary particle due to its small interaction cross section and short lifetime of τ lepton, indicating the presence of this neutrino. Nuclear emulsion technology and usage of scanning systems[1], developed during last years in the DONUT[2], CHORUS[3] and OPERA[4] experiments, allow detecting ν_τ with low background level, giving the possibility of measuring ν_τ cross section. For the first time ν_τ was detected in the DONUT experiment, where it was produced in decays of charmed mesons, namely D_s. High-energy protons were sent to a target, creating D_s mesons. These then decay in a chain, $D_s \rightarrow \tau\nu_\tau$, $\tau \rightarrow \nu_\tau X$, producing ν_τ and $\bar{\nu}_\tau$ with every $D_s \rightarrow \tau$ decay. The main source of error in measuring DONUT's ν_τ cross section is a systematic uncertainty, whereas 33% of the relative uncertainty is due to the limited number of detected ν_τ events (9 in total). The systematic uncertainty is much larger than 50% and comes from the ν_τ flux prediction. Indeed, owing to the lack of accurate measurements of the D_s differential production cross section, the DONUT result was not a single value but a ν_τ cross section as a function of a parameter n, which is responsible for the differential production cross section of D_s, as $\sigma_{\nu_\tau}^{const} = 2.51\mathrm{n}^{1.52} \cdot 10^{-40}$ cm^2 GeV^{-1}. Therefore, the central value of the ν_τ cross section was not defined (as shown in Figure 1). The cross section can be calculated only if DONUT used a parameter value derived from PYTHIA 6.1[5] simulations, as shown in Figure 1. Since the non-universality effect can be in the range of 20%–40%, reducing the error of the ν_τ cross section from its current value ($> 50\%$) to 10% would be a valuable result. Precisely measuring the cross section would enable testing lepton universality in ν_τ scattering and it also has practical implications for neutrino oscillation experiments and high-energy astrophysical ν_τ observations.[6]
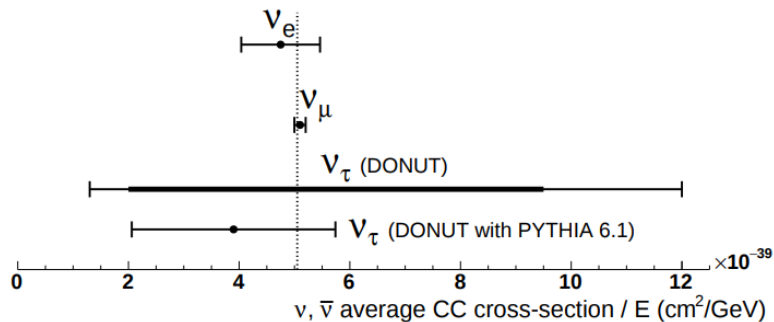
Figure 1: ν, $\bar{\nu}$ averaged energy independent cross section of three neutrinos. The vertical dashed line shows the Standard Model prediction.[6]

1 DsTau experiment

1.1 Physics motivations

The DsTau experiment aims to study tau-neutrino production in 400 GeV/c proton interactions. The outcome of this experiment is prerequisite for measuring the ν_τ charged-current cross section that has never been measured well. D_s mesons, the source of tau neutrinos, following high energy proton interactions will be studied by a novel approach to detect the double-kink topology of the decays $D_s \to \tau \nu_\tau$ and $\tau \to \nu_\tau X$. Directly measuring $D_s \to \tau$ decays will provide an inclusive measurement of the D_s production rate and decay branching ratio to τ. This experiment aims to collect $4.6 \cdot 10^9$ protons on target (POT), $2.3 \cdot 10^8$ proton interactions are expected in tungsten target. In total, about 1000 $D_s \to \tau$ events will be detected, which will allow to study the differential production cross section of D_s mesons. In addition, the analysis of $2.3 \cdot 10^8$ proton interactions, combined with the expected high yield of 10^5 charmed decays as by-products, will enable the extraction of additional physical quantities.

The data obtained in this experiment will enable the ν_τ cross section from DONUT to be re-evaluated, and this should significantly reduce the total systematic uncertainty. Furthermore, these results will provide essential data for future ν_τ experiments such as the ν_τ program in the SHiP project[7] at CERN. Also, the anticipated results on tau neutrino production in proton-nuclear collisions and their interaction cross section will help planning future neutrino experiments such as DUNE[8] and HyperKamiokande[9].

1.2 Experimental setup

The double decay, studied in this experiment, occurs within ~ 5 mm from primary proton interaction. The challenge of this measurement is the detection of the one tiny kink angle of the $D_s \to \tau$ decay, which has a mean value of 7 mrad. For this purpose, emulsion detectors with nanometric precision readout are used. The emulsion detector has a position resolution of 50 nm, which leads to an intrinsic angular resolution of 0.35 mrad with a 200-μm-thick plastic base layer (Figure 2).

The structure of the detector unit is shown in Figure 3. A 500-μm-thick tungsten target is followed by 10 emulsion films interleaved with 200-μm-thick plastic sheets which act as a decay volume for short-lived particles as well as high-precision particle trackers. This unit structure is repeated 10 times to construct a module. A so-called Emulsion Cloud Chamber (ECC), which has repeated structure of emulsion films interleaved with 1-mm-thick lead plates, follows for momentum measurement of the daughter particles. Momenta of the reconstructed tracks will be determined by Multiple Coulomb Scattering (MCS) in the ECC. Three additional emulsion films will be placed upstream to tag the incoming protons. A single module is 12.5 cm wide, 10 cm high and 8.6 cm thick (for a total of 129 emulsion films). In total 370 modules will be exposed and analyzed during the experiment.[6]

Two test beam campaigns were performed in November 2016 and May 2017 at the CERN SPS. The upper left panel of Figure 4 shows the detector setup at the beamline. Each module contains extremely high track density of $O(10^5 - 10^6)$ protons/cm^2. An example of the reconstructed data from the detector is shown in the upper right panel of Figure 4. A systematic search of the decay topologies of charmed particles was applied, and the first double charm event is shown in the lower panel of Figure 4, proving that analyses of short-lived particles in actual experimental conditions are possible. The pilot run was performed in August 2018, where 30 detector modules were exposed, which is about 10% of the full statistics. This is primarily intended to provide a test of large data taking and an estimation of the background, but that also allows to re-evaluate the ν_τ cross section measured by DONUT with significantly reduced overall systematic uncertainty. The rest of statistics will be collected in 2021.

1.3 Event selection criteria

The detection efficiency was estimated to be 20% using a PYTHIA 8.1 simulation, which required the following preliminary criteria to be fulfilled: (1) the parent has to pass through at least one emulsion film (two sensitive layers), (2) the first kink daughter has to pass through at least two sensitive layers and the kink angle is ≥ 2 mrad, (3) the path length of the parent and the first kink daughter has to be < 5 mm, (4) the second kink angle is ≥ 15 mrad and (5) the partner of the charm pair is detected with 0.1 mm$\leq$flight length< 5 mm (they can be charged decays with a kink angle > 15 mrad or neutral decays). The lower angle limit is caused by scanning resolution. Table 1 shows the breakdown of the efficiency estimation. The main background source comprises hadronic secondary interactions. These can be reduced by requesting the absence of nuclear fragments (either in the backward or forward hemisphere).
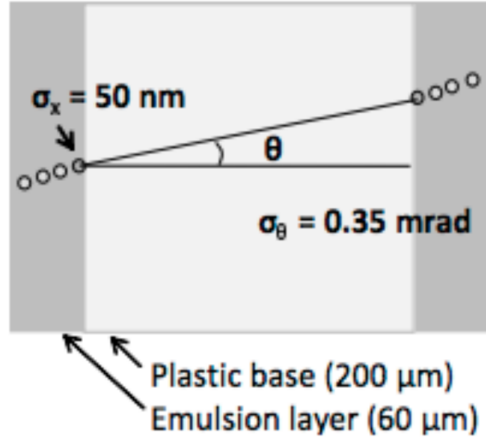
Figure 2: Schematic view of the angular measurement in an emulsion film. An angular precision of 0.35 mrad can be achieved by a single emulsion film. [10]
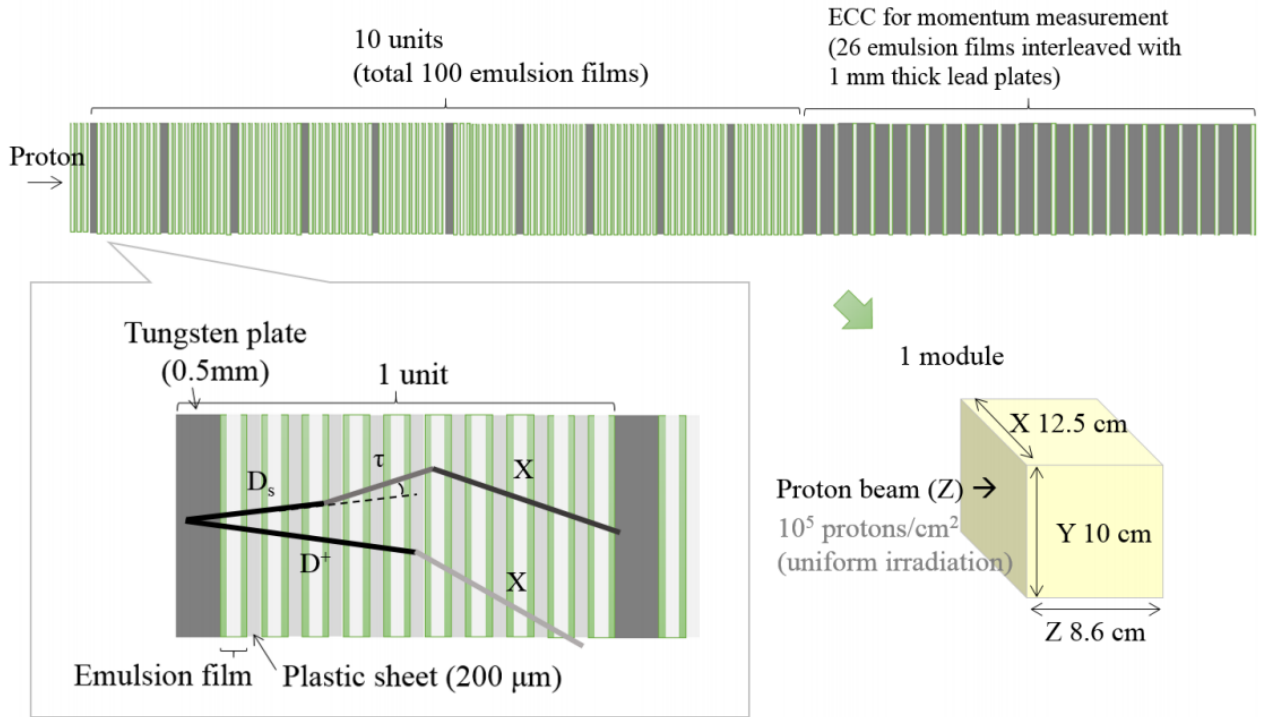
Figure 3: Schematic of the module structure. A tungsten plate, the proton interaction target, is followed by 10 emulsion films and 9 plastic sheets as a tracker and decay volume. The sensitive layers of emulsion detectors are indicated in green. This structure is repeated 10 times; then, a so-called Emulsion Cloud Chamber (ECC) structure follows for momentum measurement of the daughter particles. [6]

Table 1: Breakdown of the efficiency estimation. [6]

Selection	Total efficiency (%)
(1) Path length of $D_s \geq 2$ emulsion layers	77
(2) Path length of $\tau \geq 2$ emulsion layers and $\Delta\theta D_s \to \tau \geq 2$ mrad	43
(3) Path length of $D_s < 5$ mm and flight length of $\tau < 5$ mm	31
(4) $\Delta\theta\tau \to X \geq 15$ mrad	28
(5) Pair charm: 0.1 mm$\leq$ path length< 5 mm	20
(charged decays with $\Delta\theta \geq 15$ mrad or neutral decays)	
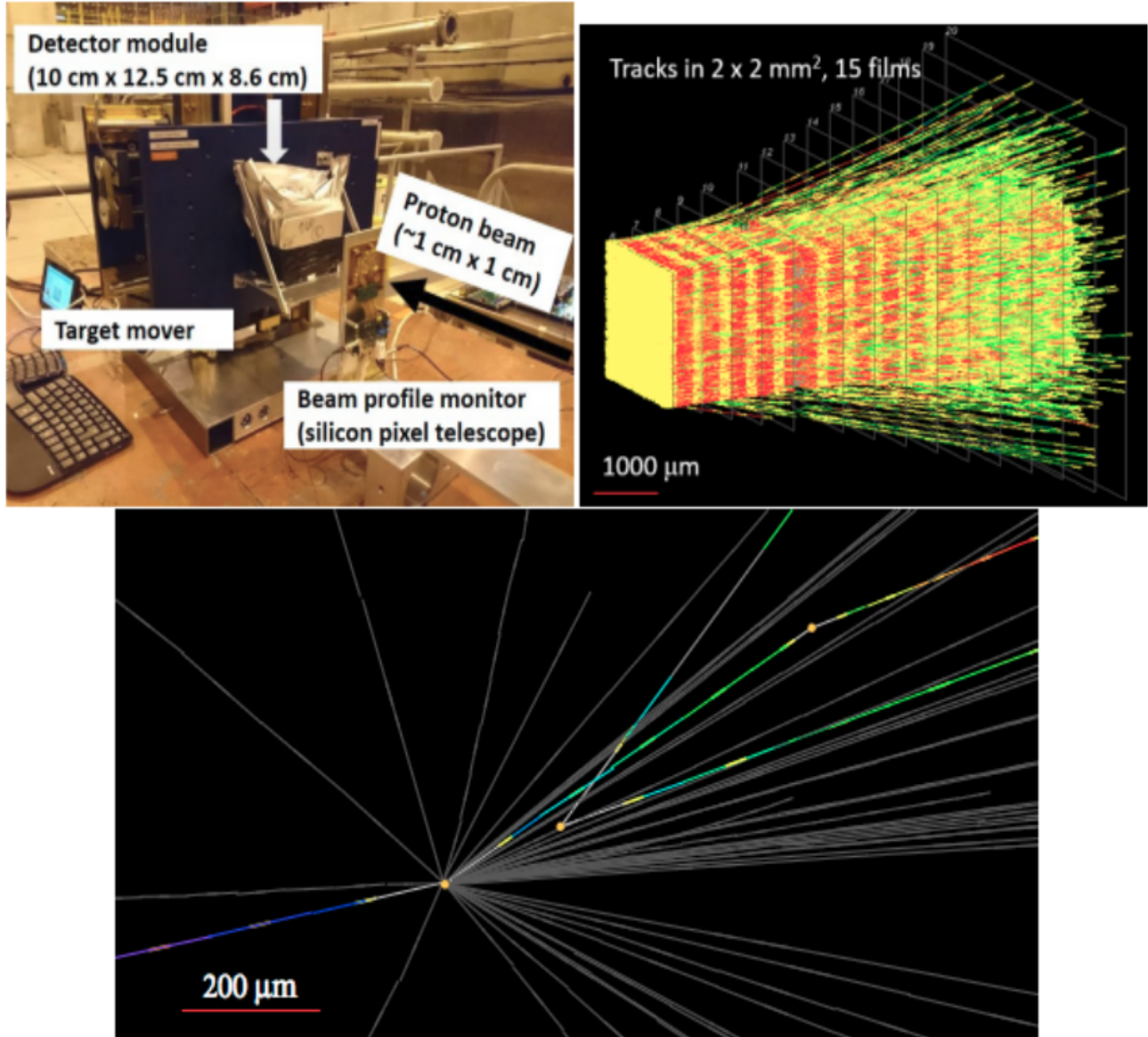
Figure 4: Top-left: Photo of the detector setup for the test beam campaign at the CERN SPS H4 beamline. The detector module was driven by a target stage so that it was uniformly exposed to the proton beam at a density of 10^5 protons/cm^2. Top-right: An example of the track data reconstructed in 2×2 mm^2 and 15 films. About 15000 tracks are reconstructed in this volume. Bottom: A double charm event with a neutral 2-prong (vee) and a charged 1-prong (kink) topology (tilted view). [10]

4

2 Data and MC comparison

The main aim of the DsTau experiment is the search for double-kink $D_s \to \tau$ topology, and the extended program involves extraction of additional physical quantities such as the interaction length of charmed hadrons, the Λ_c production rates and the search of super-nuclei. The main source of background mimicking charm decays are secondary hadronic interactions and multiple scattering. In this section hadron data from Monte-Carlo modeling is compared with the experimental pion beams data[11] in order to conclude if the simulated data is in agreement with the reconstructed data, or if the reconstruction procedure affects background evaluation and should be taken into account.

2.1 π^- selection

For this analysis the data obtained during an ECC block exposure to 2, 4 and 10 GeV/c pion beams[11] and FLUKA-based simulation[12] in DsTau module are used. The FLUKA data, corresponding to $3 \cdot 10^5$ POT, is stored in three trees: one with information about primary proton beam, another one with the MC-truth parameters of all interactions and decays, and the last one contains the detector response. This comparison was done using data from the second tree to check only MC-true interactions and to avoid uncertainties, related to reconstruction algorithms. The tree contains information about every interaction vertex: it's position (three coordinates), a region where the interaction occurred (emulsion, plastic, lead, tungsten) and whether it's a primary proton interaction, a secondary or higher order interaction or a decay of a charmed particle. The information about interacting (parent) and all interaction products (daughter particles), namely FLUKA id, energy and directional cosines, is also stored in the tree.

The angle and momenta distributions of secondary π^- interactions, which occurred in ECC part ($Z > 5.3$ cm), are shown on Figure 5 a) and b), respectively. To reproduce the data, the forward π^- with the angular acceptance $\tan\theta < 0.1$ with respect to the z-axis are selected, momenta distributions of the π^- interacted in Pb and in emulsion/plastic plates with this selection criteria are shown on Figure 5 c) and d), respectively. The 1 GeV/c width intervals around 2, 4 and 10 GeV/c were selected. For each energy interval the number of interactions in this interval is of $10^3 - 10^4$ order.
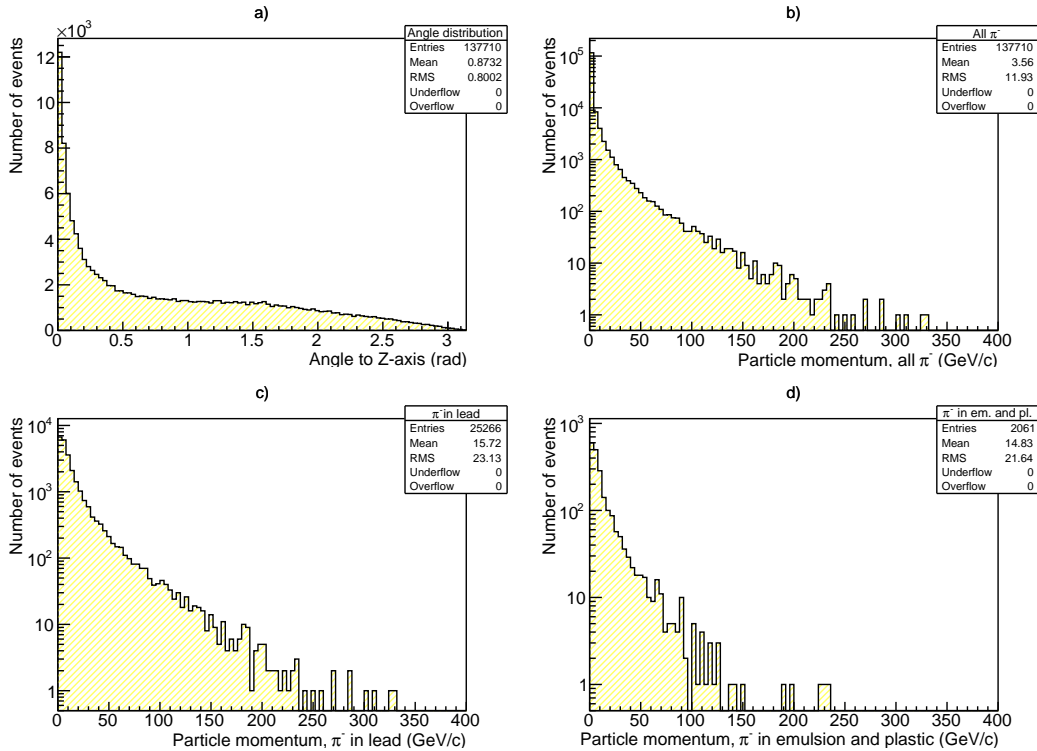
Figure 5: a) and b) Angular and momenta distributions of all π^- interacted in ECC; c) and d) Momenta distribution of forward π^- with $\tan(\theta < 0.1)$ interacted in lead (c) and emulsion/plastic plates (d) in ECC.

2.2 Interaction length

The interaction length is calculated as follows:

$$\lambda = -\frac{L}{ln(1 - \frac{N}{N_0})},$$

where L is the thickness of a lead plate and an emulsion film (L = 1300 μm), N is the number of secondary interactions and N_0 is the sum of the numbers of followed tracks in all analyzed films ($N_0 = \frac{Total\ Track\ Length}{L}$).

Total track length is the sum length of all π^- tracks in ECC, only pions born in primary proton interactions are used. A parent π^- in secondary interaction can be a daughter of primary or secondary (third order, ...) interaction, but the Monte-Carlo data format does not provide a way to determine if the interacting π^- originates from primary vertex or not. So, in order to evaluate N and *Total Track Length* an algorithm, which determines if a π^- from primary interaction interacted or exited ECC without interactions was devised. It exploits angles, energies and impact parameter in order to match an interacting π^- with one of daughter π^- in another interaction to determine which interaction the particle originates from (see Appendix 1 for more information).

The statistics of the interaction measurements are summarized in Table 2 and evaluated interaction lengths are presented. Figure 6 shows momentum dependence of the interaction length.

Table 2: Results of the interaction measurements[11] and of the simulated DsTau data (MC) analysis. Number of tracks followed, total track length followed in the ECC, number of interactions in the ECC, evaluated interaction length, λ, for each momentum beam are presented.

P[GeV/c]	2	2(MC)	4	4(MC)	10	10(MC)
Tracks	584	15366	913	17040	2205	7911
Total L [mm]	8506	354485	12620	399043	38534	186573
Interactions	77	1987	68	1752	173	793
λ [mm]	$109.8^{+14.1}_{-11.4}$	$177.8^{+3.9}_{-4.1}$	$184.9^{+24.2}_{-20.1}$	$227.1^{+5.3}_{-5.6}$	$222.5^{+18.4}_{-15.8}$	$234.6^{+8.1}_{-8.7}$
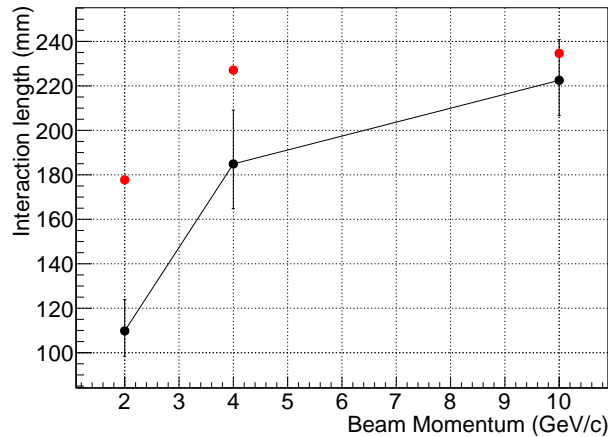
Figure 6: Interaction length as a function of beam momentum. Black dots with error bars and red circles show experimental data and simulated data, respectively.

2.3 Topological characteristics

The multiplicity and kink angle distributions of relativistic charged secondary particles are shown in Figures 7 and 8. Topological characteristics are summarized in Table 3 and they are compared with those of simulated data.

Two different methods to determine whether the particle is a nuclear fragment or a relativistic particle were used. In the first one, the particles with FLUKA $id \leq 0$ are considered heavy, others are relativistic particles (hereinafter referred to as "id" method). In the second one, a particle is considered heavy if it has $\beta < 0.7$ and

6

$mass \geq proton\ mass$ or it has FLUKA $id \leq 0$ (hereinafter referred to as "β" method). In the beam data analysis the second method was applied, β was calculated using multiple scattering. Angular selection criteria for MIP – $\tan\theta < 0.6$ and $\tan\theta < 3.0^{13}$ for heavy (derived from scanning system limits).
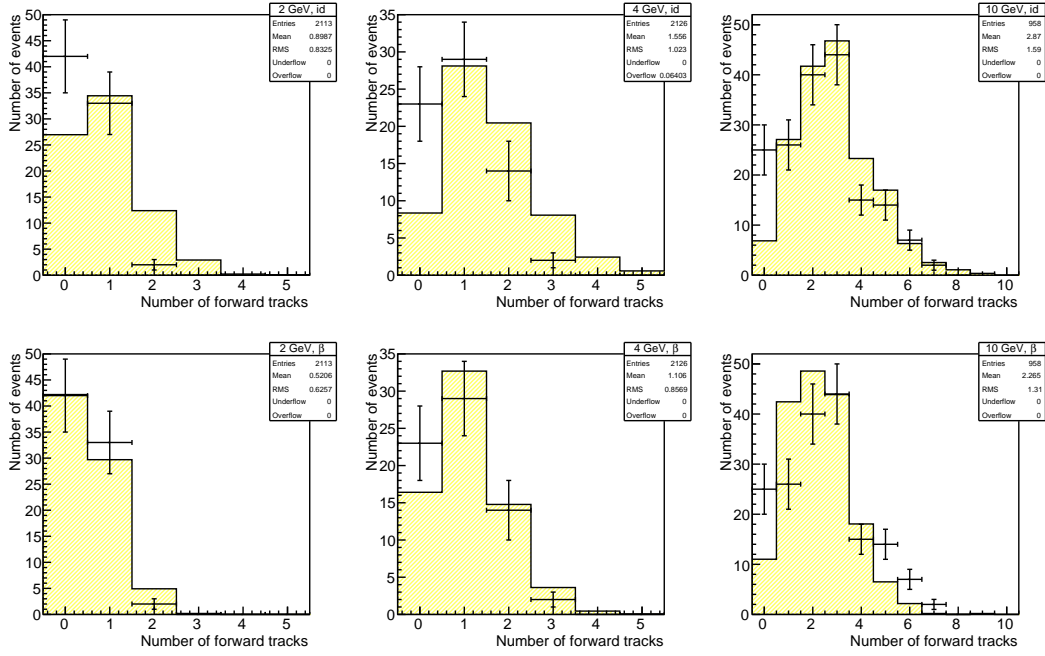
Figure 7: Multiplicity distributions of relativistic particle tracks in the forward hemisphere using id method (Top) and β method (Bottom) to identify nuclear fragments for experimental data (dots with error bars) and simulated data (histogram). The simulated distributions are normalized to the real data.
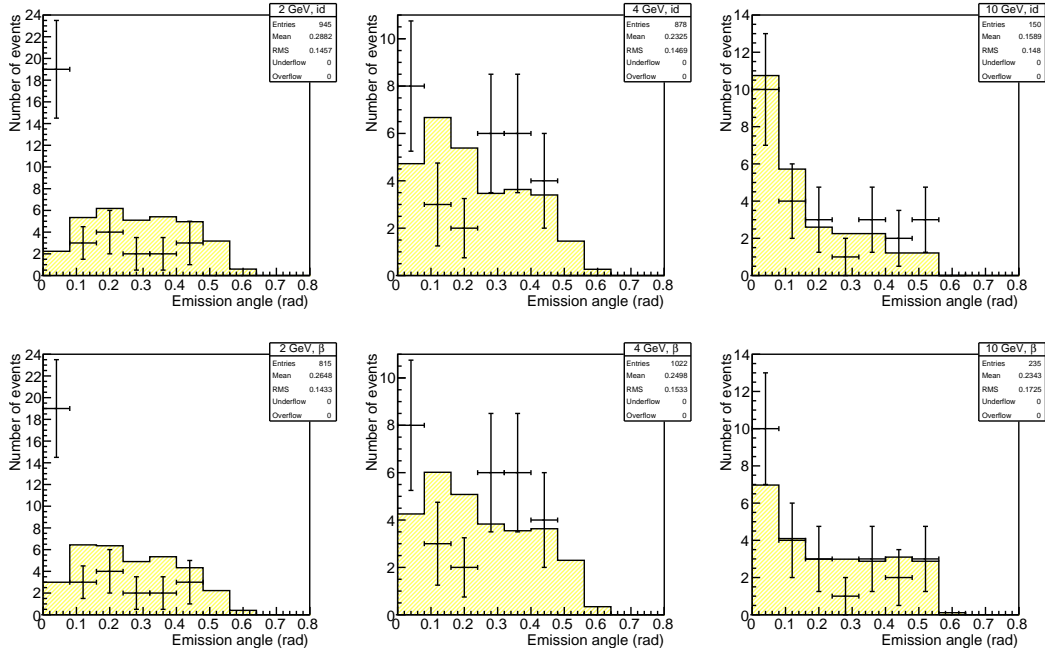
Figure 8: Kink angle distributions of 1-prong events using id method (Top) and β method (Bottom) to identify nuclear fragments for experimental data (dots with error bars) and simulated data (histogram). The simulated distributions are normalized to the real data.

7

Table 3: Topological characteristics of experimental data and simulated data (MC). In MC columns the numbers not in brackets (in brackets) were obtained using β (id) method. Number of events, average charged particle multiplicity $<n>$, number of 1-prong events, average kink angle for 1-prong events $<\theta_{kink}>$ for 2, 4, 10 GeV/c π^- interactions are summarized.

P[GeV/c]	2	2, MC	4	4, MC	10	10, MC
Events	77	2113 (2113)	68	2126 (2126)	173	958 (958)
$<n>$	0.48	0.52 (0.90)	0.93	1.09 (1.56)	2.45	2.24 (2.87)
1-prong events	33	808 (945)	29	1025 (878)	26	238 (150)
$<\theta_{kink}>$ [rad]	0.13	0.26 (0.29)	0.23	0.25 (0.23)	0.20	0.24 (0.16)

2.4 Nuclear fragment association

The presence of nuclear fragments in an event indicates that it is a hadron interaction, which allows to reduce background. A comparison of association probability, multiplicity and angle distributions of nuclear fragments has been done in order to determine if the MC data is correct.

Measurement results of nuclear fragments for 1-prong and 3-prong π^- interactions, which are relevant to topologies of the $D_s \to \tau$ decay, and corresponding results for simulated data are presented in Table 4. Figure 9 shows the association probability as a function of the beam momentum, where data of 1-prong and 3-prong events are merged, together with simulation results. Figures 10 and 11 show multiplicity and polar angle distributions of nuclear fragments.

Table 4: Results of nuclear fragment search (experimental data and simulated data). In MC lines the numbers were obtained using β (id) method.

P[GeV/c]	2		4		10	
Prong	1	3	1	3	1	3
Events	32	0	29	2	25	41
Fragment associated	10	0	16	2	15	27
Probability [%]	$31.3^{+9.1}_{-6.9}$	-	$55.2^{+8.6}_{-9.3}$	> 46.5	$60.0^{+8.9}_{-10.2}$	$65.9^{+6.5}_{-8.0}$
Events (MC)	815 (945)	5 (80)	1022 (878)	113 (252)	235 (150)	243 (259)
Fragment associated (MC)	536 (370)	5 (46)	730 (334)	77 (136)	180 (58)	176 (139)
Probability (MC) [%]	66 (39)	100 (58)	71 (38)	68 (54)	77 (39)	72 (54)
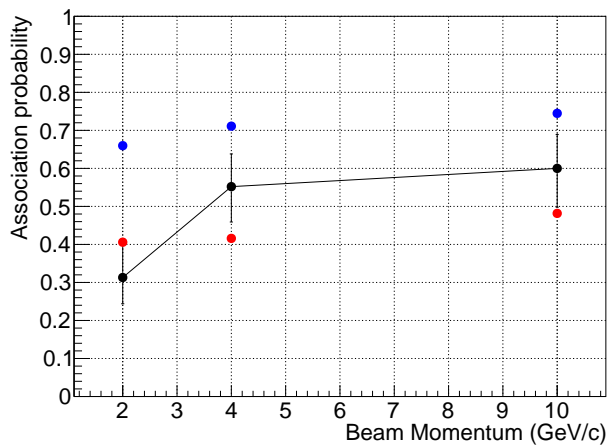
Figure 9: Association probability of nuclear fragments as a function of beam momentum. Black dots with error bars show experimental data, blue and red circles show simulated data, for those nuclear fragments are identified using β and id methods, respectively.
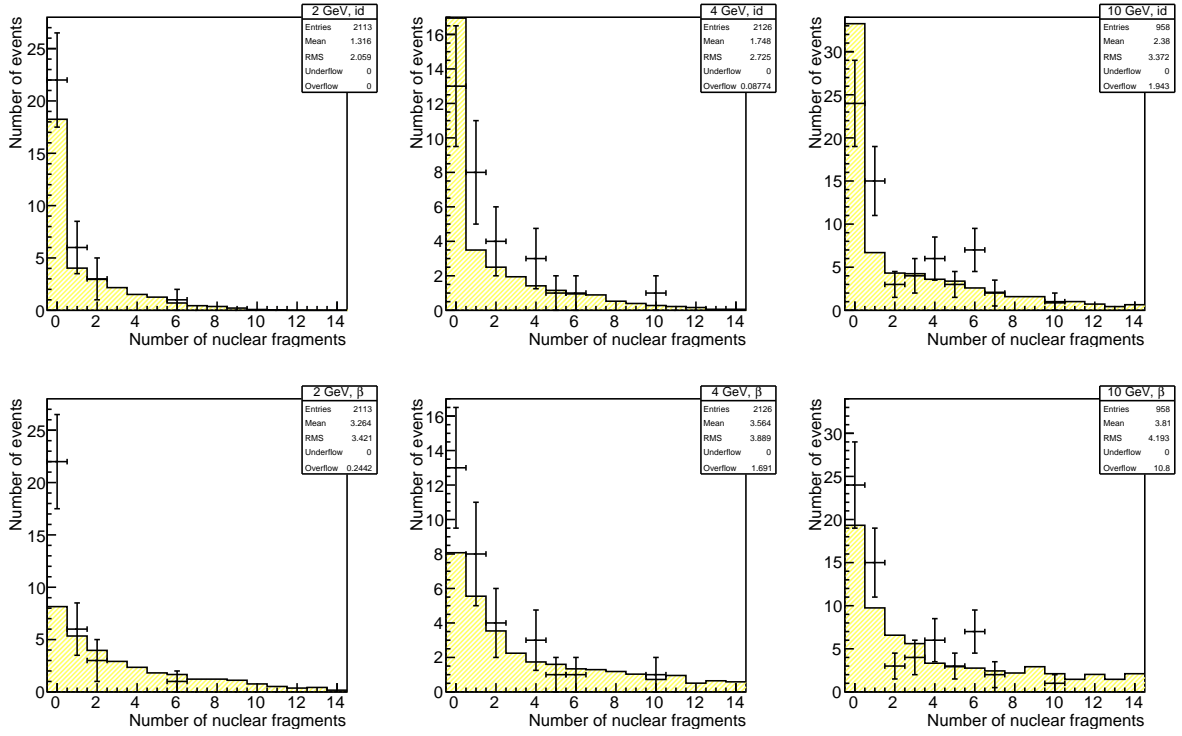
Figure 10: Multiplicity distributions of nuclear fragments for experimental data (dots with error bars) and simulated data (histogram). On top and bottom plots *id* and *β* methods are used for identification of nuclear fragments, respectively.
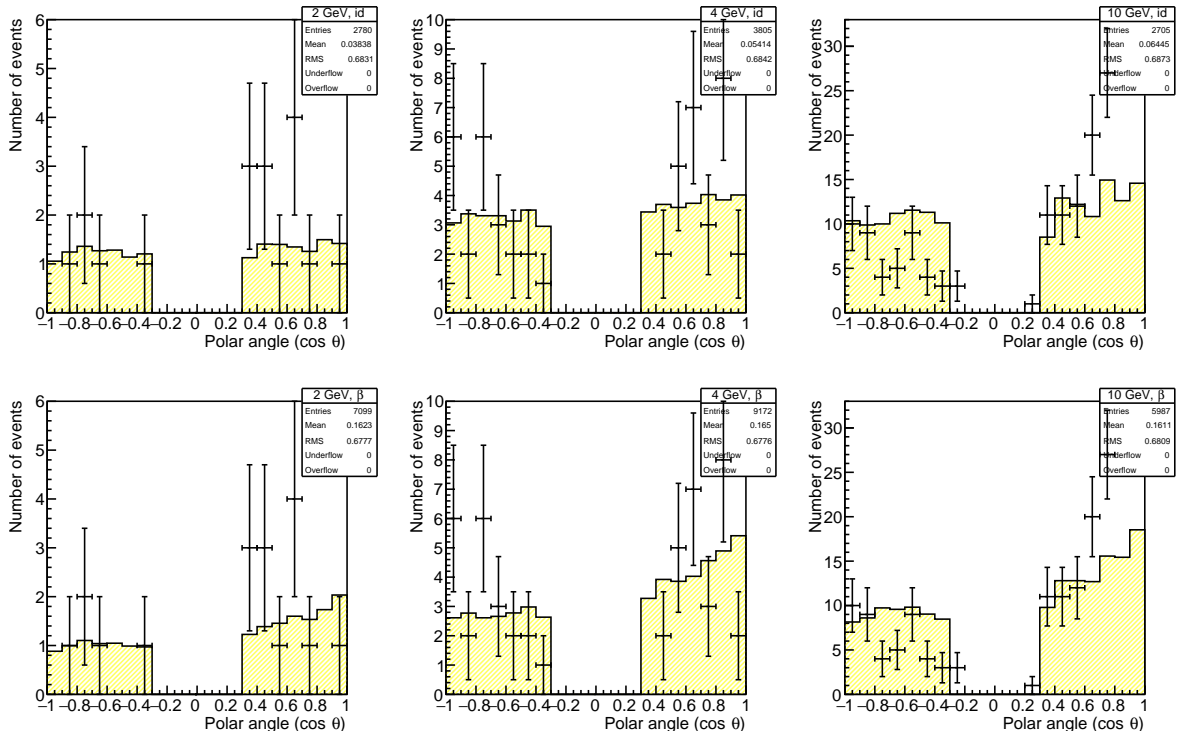
Figure 11: Polar angle distributions of nuclear fragments for experimental data (dots with error bars) and simulated data (histogram). On top and bottom plots *id* and *β* methods are used for identification of nuclear fragments, respectively.

3 Background evaluation

To evaluate background, hadronic decays or interactions mimicking DsTau experiment signal topology, shown in Figure 3, need to be found. The background event has to contain an interaction, similar to $D_s \to \tau \to X$, and another interaction, similar to $Charm \to X$. This charm is hereinafter called the "pair-D". So, background comes from primary proton interactions with at least two daughter hadrons, both interacting within several millimeters from the primary vertex, one having 1-prong topology (looks like $D_s \to \tau$) and it's daughter having similar topology (looks like $\tau \to X$). The probability of a background event occurring is calculated as follows:

$$P_{Bg}^{tot} = P_{Bg}^{D_s \to \tau} * P_{Bg}^{\tau \to X} * P_{Bg}^{pair-D}$$

where $P_{Bg}^{D_s \to \tau}$ is the probability of mimicking a $D_s \to \tau$, $P_{Bg}^{\tau \to X}$ is for $\tau \to X$ and P_{Bg}^{pair-D} is the probability of mimicking pair-D topology.

3.1 Preliminary selection criteria

At first, selection criteria, used for preliminary signal selection, are applied in order to estimate background. The angular criteria have been tuned since the beginning of the experiment and are slightly different from those in Table 1. The angular selection criterion 0.002 rad$< \theta_{kink} < 0.03$ rad is used to determine if a hadron interaction mimics the $D_s \to \tau$ decay. The upper limit is selected in accordance with angular distribution, shown in Figure 12. The angular selection criterion 0.02 rad$< \theta_{kink} < 0.5$ rad and path length criterion 0.1 mm $<$ path length < 5 mm are applied for mimicking the pair-D particle decay, as well as τ decay. The number of hadronic events is calculated for all combinations of selection criteria and three different parent momentum selection criteria. The results are presented in Table 5, only events without heavy fragments (determined using id method) were counted. For further calculations a $P_{par} \geq 2$ GeV/c selection criterion is selected. It was estimated that this selection criterion suppresses background, while not interfering with desired events too much.
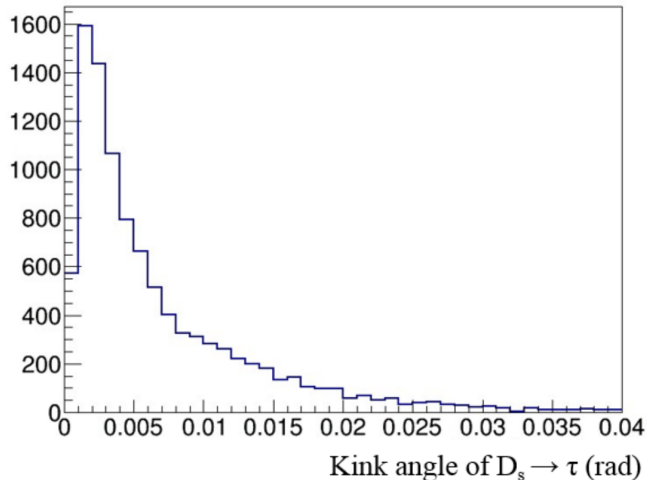
Figure 12: PYTHIA simulated $D_s \to \tau$ kink angle distribution.[6]

Table 5: Number of hadronic interactions, passed preliminary selection criteria, for $3 \cdot 10^5$ POT simulated.

	Selection	$P_{par} > 0$ GeV/c	$P_{par} > 1$ GeV/c	$P_{par} > 2$ GeV/c
(1)	0.002 rad$< \theta_{kink} < 0.03$ rad	231^{+15}_{-15}	231^{+15}_{-15}	231^{+15}_{-15}
(2)	0.002 rad$< \theta_{kink} < 0.03$ rad 0.1 mm $<$ path length < 5 mm	29 ± 5	29 ± 5	29 ± 5
(3)	0.02 rad$< \theta_{kink} < 0.5$ rad	1241^{+35}_{-35}	1205^{+34}_{-35}	1189^{+34}_{-34}
(4)	0.02 rad$< \theta_{kink} < 0.5$ rad 0.1 mm $<$ path length < 5 mm	189 ± 14	183 ± 14	180 ± 13
(5)	0.1 mm $<$ path length < 5 mm	211 ± 14	205 ± 14	202 ± 14

Total amount of primary protons in MC data is $3 \cdot 10^5$, however $4.6 \cdot 10^9$ will be collected during the actual experiment. If only angular criteria are applied: $P_{Bg}^{D_s \to \tau}$ is calculated using preliminary selection criterion (1), and $P_{Bg}^{\tau \to X}$ and P_{Bg}^{pair-D} – with selection criterion (3), the probability of a background event occurring is $(1.21 \pm 0.04) \cdot 10^{-8}$ and (55.6 ± 1.7) background events are expected in full statistics. A combination of angle and path length criteria: (2) and (4) for $P_{Bg}^{D_s \to \tau}$ and for $P_{Bg}^{\tau \to X}$ and P_{Bg}^{pair-D}, respectively, gives the probability of a background event occurring is $(3.5 \pm 0.2) \cdot 10^{-11}$ and the expected number of background events reduces to (0.160 ± 0.011). For this two cases the background level is at the order of $\sim 1\%$ or even less, which means that selection criteria, used for the main analysis could be wider in order to increase signal detection efficiency.

On the other hand, the extended analysis in this experiment involves charm characteristics study, kink angle versus path length distribution for charged charmed particles and background hadrons is presented in Figure 13. Green vertical lines represent angular selection criteria for pair-D. It is noticeable that a large amount of background events pass those criteria. Horizontal green lines in Figure 13 represent path length selection criteria, which suppress hadronic background, but significantly reduce charm signal level.

Efficiency represents the ratio of selected charm events to all such events. Purity shows the amount of signal events among all selected events. They are determined as follows:

$$\text{Efficiency} = \frac{N_{selected\ charm}}{N_{all\ charm}}, \quad \text{Purity} = \frac{N_{selected\ charm}}{N_{all\ selected}}.$$

The (3) selection criterion for pair-D gives 83% efficiency and 5% purity. With criteria (4) applied, the purity level increases to approximately 20%, however efficiency decreases to only 60%.

The signal area in Figure 13 has a complex shape and can not be selected with straight selection criteria with high efficiency and purity levels at the same time. For this reason likelihood approach was tested for signal/background determination. It is described in the next subsection.
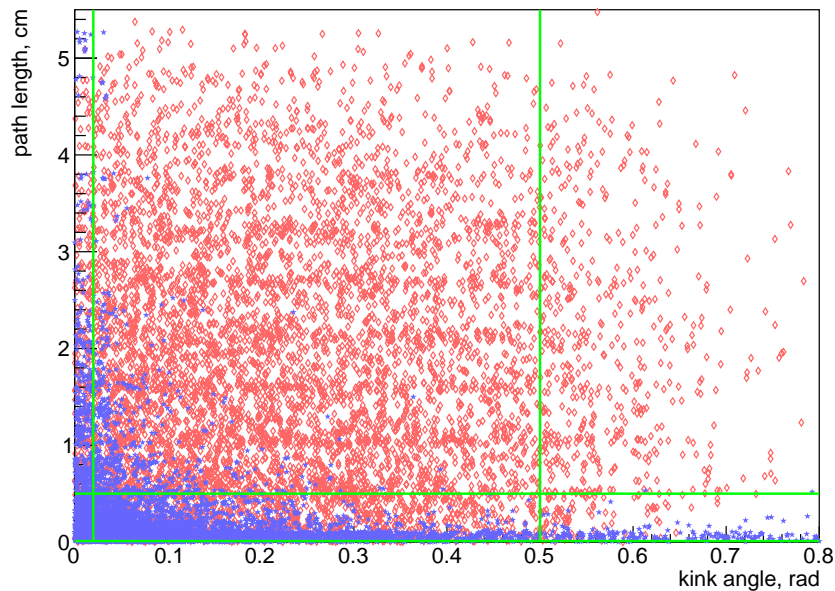
Figure 13: Kink angle versus path length for hadrons (red) and for charmed particles (blue). Green lines stand for applied straight selection criteria.

3.2 Likelihood selection criteria

The likelihood as a function of θ_{kink} and l_{path} is used to achieve better hadron/charm separation. It is defined as

$$Lh(\theta_{kink}, l_{path}) = ln \frac{P(\theta_{kink}, l_{path}|D)}{P(\theta_{kink}, l_{path}|H)},$$

where $P(\theta_{kink}, l_{path}|D) = \dfrac{N_D}{N_D + N_H}$ $\left(P(\theta_{kink}, l_{path}|H) = \dfrac{N_H}{N_D + N_H} \right)$ is the probability of an event with certain kink angle and path length being charm decay (hadronic interaction). D and H represent charmed particles and hadrons, respectively. Higher likelihood value corresponds to higher probability of finding a signal event. Histograms with likelihood function for both hadronic interactions and charm decays, as well as histograms with efficiency and purity are shown in Figure 14. More details about likelihood calculations are in Appendix 2.
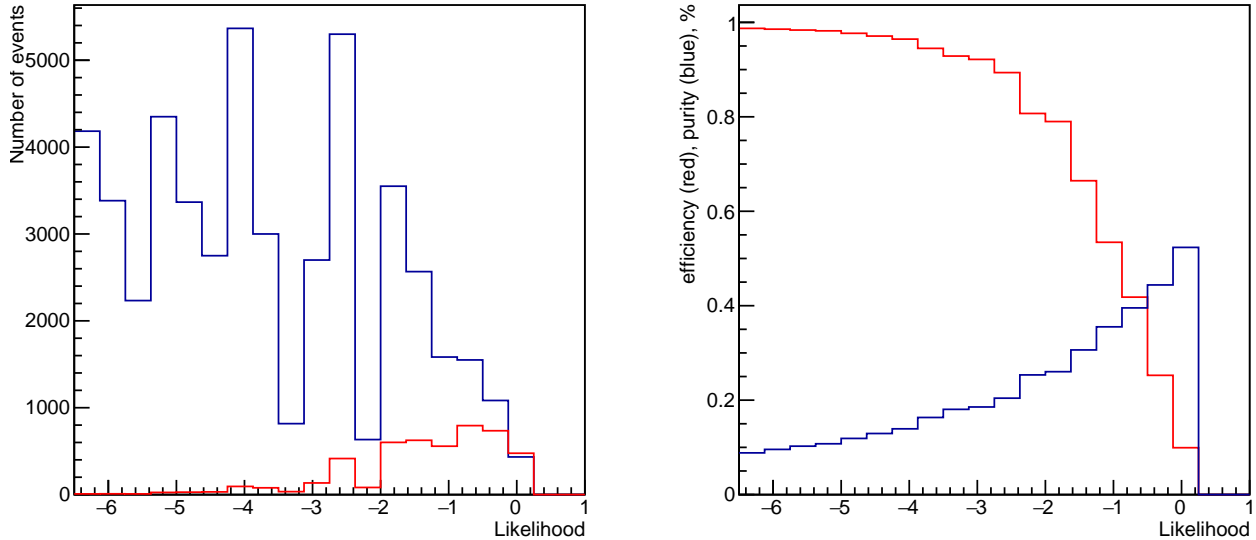
Figure 14: Left: Likelihood function for hadronic (blue) and charmed (red) events. Right: Efficiency (red) and purity (blue) as functions of likelihood.

$Lh \geq -2.45$ corresponds to 83% efficiency of pair-D detection (like with only angle selection criteria), however the probability of a background event occurring is $(3.2\pm0.9)\cdot10^{-10}$, total amount of background events is (1.5 ± 0.4).

$Lh \geq -1.38$ corresponds to 60% efficiency of pair-D detection (like angle and path length selection criteria), the probability of a background event occurring is $(2.1\pm0.7)\cdot10^{-11}$, total amount of background events is (0.10 ± 0.03).

4 Results and discussion

The interaction lengths for 4 and 10 GeV/c are consistent with the pion beam data. For 2 GeV/c the interaction length and kinematical characteristics are different from those in the article. The probable reason could be identification of multiple scattering as a 1-prong interactions with no nuclear fragments in the measurements. This method provides lower ratio of events without nuclear fragments, while the β method provides a higher ratio. Therefore the id method is used for background evaluation, since it gives a slightly overestimated background. The difference between data and Monte-Carlo may come from reconstruction uncertainties. That should be studied more carefully to achieve better agreement.

The background is evaluated using preliminary selection criteria, which gives background suppression to the level of $\sim 1\%$ for the main aim of the experiment, although it does not reduce background well for the extended charm analysis. Using likelihood method allows to maintain high signal efficiency with higher purity for charm analysis. It gives 1.6 times less background with the same charm detection efficiency, which provides a possibility to increase signal detection efficiency for the main analysis, keeping the same background value. The likelihood method gives background event occurring probability $(2.1 \pm 0.7) \cdot 10^{-11}$ and total amount of background events is (0.10 ± 0.03). The efficiency of the charmed particle track identification is 60%, the purity is 32%, whereas straight selection criteria with such efficiency provide only 20% purity.

In this study only background from 1-prong hadronic events was estimated. Further work should be done for evaluating background from 3-prong hadron interactions. Also only charged pair-D particle case was examined, the

background for topology with neutral pair-D should also be estimated. As should be the background for other tau decay channels (only 1-prong was examined during this work). Background from other charmed particles mimicking the $D_s \to \tau$ decay is also a crucial value for this experiment. More study to be done in this direction.

5 Acknowledgements

Appendix 1. The method of tracks matching

The following algorithm is applied to evaluate the total track length (the algorithm scheme is shown in Figures 15, 16):

- Each parent π^- of secondary interaction is compared with all daughter π^- from primary and secondary interactions to find a best corresponding track and to define whether it originates from the primary interaction or not

- If a parent π^- originates from the primary vertex, a part of the path length between the primary and secondary vertices, which is located in ECC, is added to the total track length

- If no match is found for a daughter π^- from primary proton interaction, which passes the selection criteria, its track is extrapolated to the point, where it exits the detector. The paths of these π^- in ECC are also added to the total track length

The criteria of comparison are the energy difference, track directions and the impact parameter of the parent track to the primary and secondary vertices. The correspondence search is an iterative procedure and the parameters of the first iteration are:

- Impact parameter ≤ 0.06 cm (see Figure 17)

- $0 \leq \Delta$ Energy ≤ 0.05 GeV – the energy difference between the parent particle in a secondary interaction and the daughter particle, which it is being matched to

- Angle between track directions in two vertices ≤ 0.08 rad

The best match is selected. If no match is found, the criteria are broadened until at least one match is found or the parameters become 10 times larger than they were in the first iteration. If a pion passes through the whole detector, it loses approximately 0.03 GeV of energy and deviates by no more than 0.04 rad due to multiple scattering. These numbers were used to select parameter values.
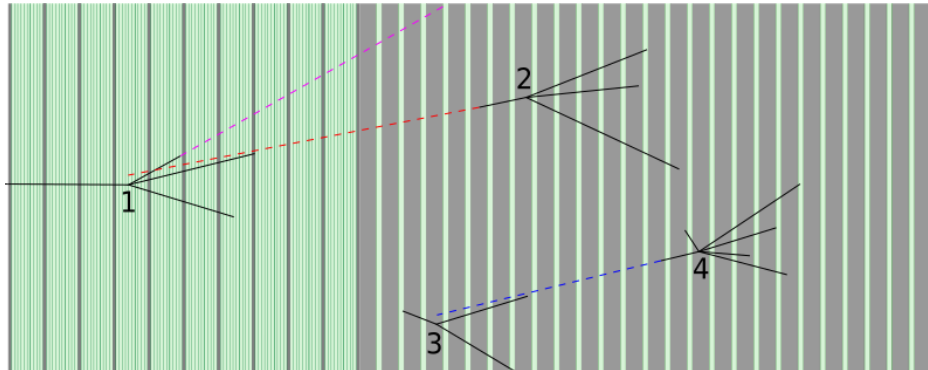
Figure 15: Schematics of tracks matching algorithm. The left part of the detector is the module, the right is ECC. Light green parts are plastic, dark green are emulsion, gray parts in ECC are lead, in module – tungsten. 1 is a primary vertex, 2 − 4 are secondary vertices. π^- born in 1 and 3 are matched with those interacting in 2 and 4.
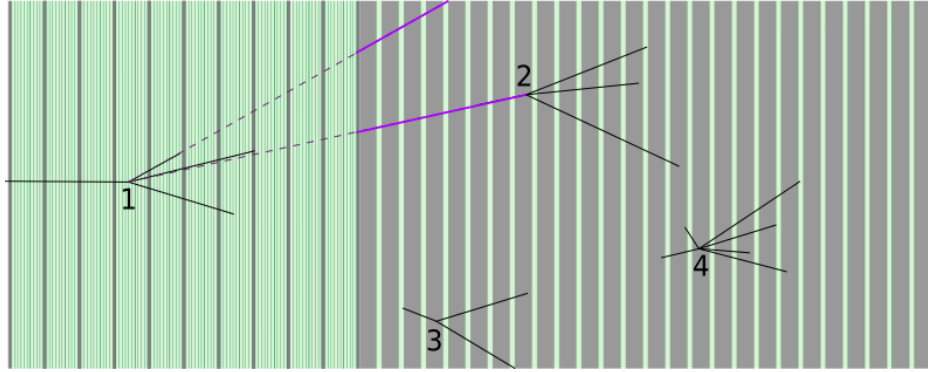
Figure 16: Schematics of the total track length evaluation algorithm. The first π^- from interaction vertex 1 doesn't interact, so it's track is extrapolated to the point of exit from the detector. The second π^- interacts in ECC, it's track is presumed to be the line segment between points 1 and 2. Purple parts of both tracks are added to the total track length.
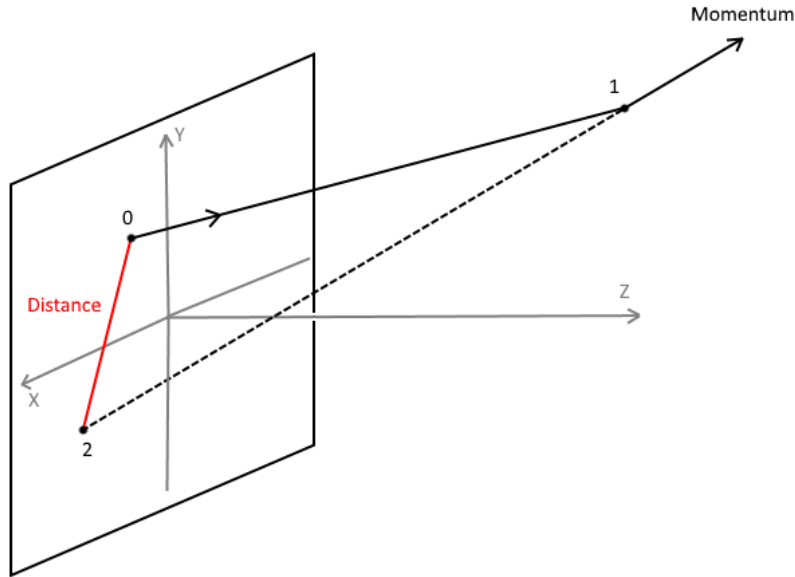
Figure 17: Impact parameter evaluation. π^- is born in point 0 and interacts in point 1. Point 2 is obtained by extrapolating momentum direction to the plane $z = Z_0$.

Appendix 2. Likelihood evaluation

Path length and kink angle are the selection criteria to determine charmed particles and hadrons. Two-dimensional histograms with constant bin size of kink angle versus path length were filled for hadrons and charmed particles, they are presented on left plots in Figure 18. After that bin sizes were adjusted, so that there were no empty bins in this histogram for hadrons in the area, where charmed particles have the highest concentration, right plots in Figure 18. The rebining is applied to avoid fluctuations in likelihood evaluation in the area with low statistics.

Likelihood distribution is presented in Figure 19. If calculating likelihood was impossible (e.g. no events in bin), likelihood value was set to -10, to be interpreted as the region with no signal. On the plots in Figure 14 the region with $Lh = -10$ is not presented since it is not the region of interest.
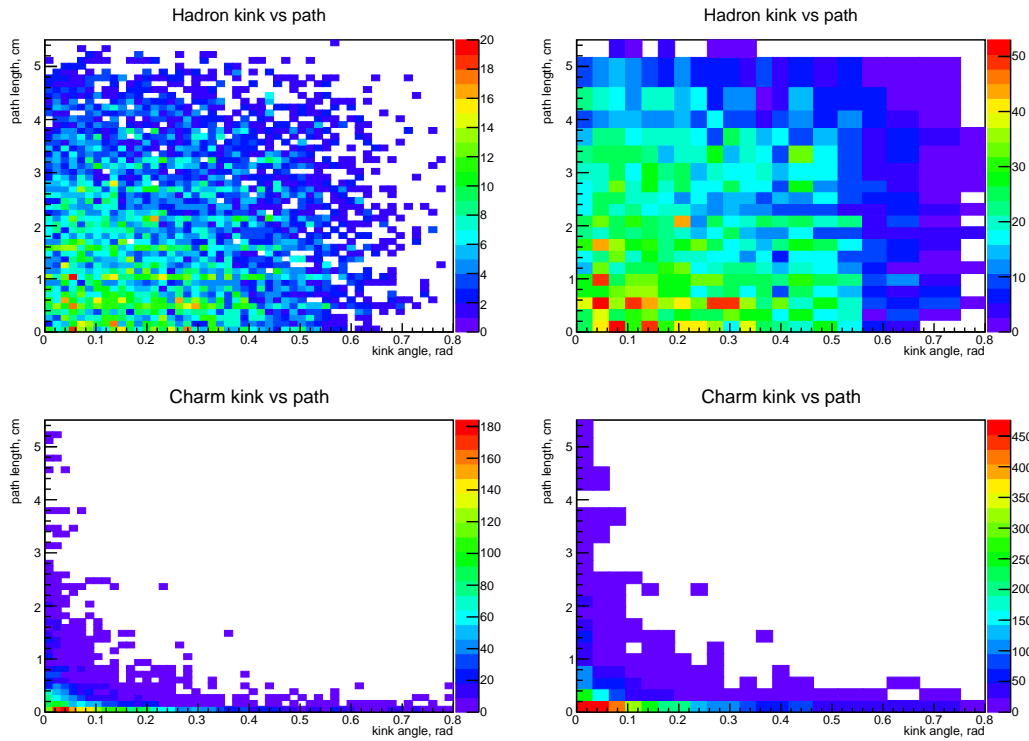
Figure 18: Kink angle versus path length for hadrons (top) and for charmed particles (bottom). Histograms with constant bin size are presented in the left column, with different bin sizes are presented in the right column.
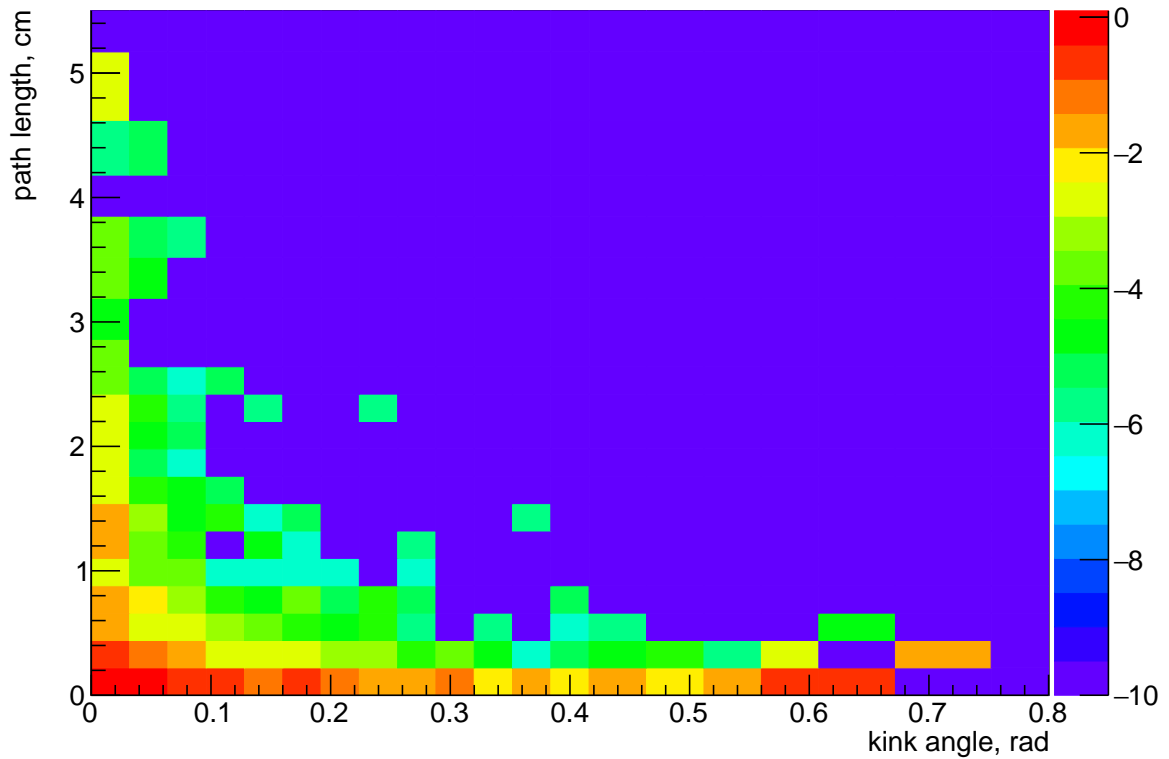
Figure 19: Likelihood distribution. Higher probability of finding a signal event corresponds to higher likelihood value.

References

[1] A. Ariga and T. Ariga, *Fast 4π track reconstruction in nuclear emulsion detector based on GPU technology*, JINST 9 (2014) P04002

[2] K. Kodama et al.(DONuT Collaboration), *Final tau-neutrino results from the DONuT experiment*, Phys. Rev. D 78 (2008) 052002.

[3] E. Eskut et al. (CHORUS Collaboration), *New results from a search for $\nu_\mu \to \nu_\tau$ and $\nu_e \to \nu_\tau$ oscillation*, Phys. Lett. B497 (2001), 8-22

[4] N. Agafonova et al. (OPERA Collaboration), *Final Results of the OPERA Experiment on ν_τ Appearance in the CNGS Neutrino Beam*, Phys. Rev. Lett., 120, 211801

[5] T. Sjostrand et al., *High- energy physics event generation with PYTHIA 6.1*, Comput. Phys. Commun. 135 (2001) 238-259

[6] S. Aoki et al. *Experiment Proposal. Study of tau-neutrino production at the CERN SPS.* arXiv:1708.08700

[7] M. De Serio for the SHiP Collaboration, *Neutrino physics with the SHiP experimentat CERN*, PoS EPS-HEP2017 (2017) 101

[8] Davide Meloni, *On the systematic uncertainties in DUNE and their role in New Physics studies*, JHEP 1808 (2018) 028, arXiv:1805.01747 [hep-ph]

[9] K. Abe et al., *Letter of Intent: The Hyper-Kamiokande Experiment*, arXiv:1109.3262v1 [hep-ex].

[10] A. Ariga and T. Ariga for the DsTau Collaboration, *Neutrinos: the hunt continues at CERN*, CERN EP Newsletter (https://ep-news.web.cern.ch/content/neutrinos-hunt-continues-cern)

[11] H. Ishida et al. *Study of hadron interactions in a lead-emulsion target.* PTEP, 2014, arXiv [1408.0386]

[12] T. T. Bhlen et al., *The FLUKA Code: Developments and Challenges for High Energy and Medical Applications*, Nucl. Data Sheets 120 (2014) 211

[13] T. Fukuda et al., *Automatic scanning of nuclear emulsions with wide-angle acceptance for nuclear fragment detection*, J. Instrum., 8, P01023 (2013).

[14] M. Tanabashi et al. *Particle Data Group*, Phys. Rev. D 98, 030001 (2018). (http://pdg.lbl.gov/)